AIAA 81-4077

Fatigue Crack Growth at Stress Concentrations Subjected to Strains beyond Elastic Range

M. M. Ratwani,* D. P. Wilhem,† J. P. Carter,‡ and H. P. Kan‡
Northrop Corporation, Hawthorne, Calif.
and
M. Kaplan§
Federal Aviation Administration, Chicago, Ill.

Fatigue crack growth data were obtained for through- and part-through-the-thickness cracks at 0.5, 1.5, and 3.0 in. (12.7, 38.1, and 76.2 mm) notch radii commonly encountered in aircraft wing structures. Nonlinear analysis of through-the-thickness cracks at notch radii was performed with the NASTRAN computer program for various crack lengths and applied stress levels. Using this elastic-plastic analysis, *J*-integral values were computed and modified stress intensity factors were obtained based on the square root of *J*. These stress intensity factors were used in combination with a crack propagation model to predict the crack growth life of the test specimens with through-the-thickness flaws. Elastic stress intensity factors corrected for plasticity have been used in the crack propagation law to predict fatigue life of specimens with part-through flaws. The plasticity correction for part-through-the-thickness flaws has been applied based on the *J*-integral values computed for through-the-thickness flaws. The analytical predictions of crack growth life show good agreement with experimental results for constant amplitude, as well as spectrum loadings.

Introduction

TYPICAL structural details in aircraft construction often incorporate fastener holes and cutouts that result in stress gradients and peak stresses much greater than the gross design stress. These stress concentrations generally represent fatigue-critical areas in aircraft structures. At these points, fatigue cracks, if not already present, initiate and propagate during flight loading. Methods of analyzing the fatigue crack growth at these locations using linear elastic fracture mechanics (LEFM) are available in the literature. Often, however, large plastic zones develop in the vicinity of these areas, invalidating the use of LEFM methods. These plastic zones result from peak stresses, at the point of stress concentration, that are greater than the yield stress, even though the remote nominal stress is a fraction of the design limit stress.

These fatigue crack growth problems may be classified in two categories. In the first category, initial flaws (part-through-the-thickness or through-the-thickness) exist at stress concentrations before the flight loads are applied. These flaws may be produced during the manufacturing or fabrication process. During service these flaws propagate within the large plastic zones associated with the stress concentration. In the second class of problems, there are no initial flaws in these highly stressed areas, but crack initiation occurs during flight loading. The surrounding material experiences several cycles of prestrain due to repeated loading and unloading prior to the initiation of a crack. The crack growth in this case takes place through material which has seen several cycles of prestrain and is therefore influenced by prestrain conditions. Different analytical techniques are required for predicting crack growth behavior for two category problems.

Received Dec. 10, 1979; revision received July 25, 1980.

*Senior Technical Specialist, Aircraft Group, Aircraft Division. Member AIAA.
†Senior Technical Specialist, Aircraft Group, Aircraft Division.
‡Senior Engineer, Aircraft Group, Aircraft Division.
§Aerospace Engineer.

Fatigue crack growth of through-the-thickness flaws at stress concentrations such as holes and circular cutouts has been investigated by Broek.[1] He observed good correlation between experimental crack growth data obtained on center-cracked and cracked-hole specimens for K_{max} values up 25 ksi $\sqrt{in.}$ (868.7 MPa $\sqrt{mm}$) in 2024-T3 aluminum. For higher K_{max} values, crack growth rates for specimens with holes were higher than those for center-cracked specimens. The applied remote stress in tests conducted by Broek was only about 11.2 ksi (77.22 MPa). At this stress, the stresses around the holes with no cracks present would be below the yield stress of the material and, hence, no significant effect of nonlinearity on crack growth is expected. Broek's results indicate that LEFM can be used only if the material is working in the elastic range.

The influence of prestrain on crack growth has been investigated by Kang and Liu.[2] They observed that cyclic prestrain increased the subsequent crack growth rate in 2024-T3 aluminum alloy. The magnitude of increase in crack growth rate was dependent on the amount of prestrain. The increase in crack growth rate due to prestrain on the 2024-T3 material has also been observed by Schijve.[3] He observed that one or several cycles of prestrain exhibited an identical increase in crack growth rate. These observations indicate that faster crack growth can be expected at stress concentrations when material yielding has taken place, as compared to when the material has remained elastic.

The problem investigated in this paper is the flawed condition at a point of stress concentration. The detail selected for analysis was a cutout in the wing root area of a high-performance jet aircraft. A stress gradient occurs in the area of the radius and the magnitude of loads are such that a plastic zone is formed in that area, even when no cracks are present. It is also assumed that initial flaws are present prior to the application of any flight loads. To account for the nonlinear material behavior, a piecewise linear analysis rigid format was used in the NASTRAN computer program. The results of this analysis were stresses and displacements from which values of the *J* integral could be calculated. Modified stress intensity factors were then derived from the *J* integral, and these stress intensity factors were used to predict the crack growth. The details of the analysis and correlation with experimental results are discussed in the following sections.

Application of the *J* Integral to Fatigue Crack Growth Prediction

The majority of crack growth models developed for metals relate the crack growth rate (da/dn) with effective stress intensity factor range (ΔK) or maximum stress intensity (K_{max}). Fitzgerald[4] recently proposed a crack growth model that has been found to predict crack growth very well. The crack growth rate is given by

$$\frac{da}{dn} = CK_{max}^{m}[(K_{max} + K_{env})(1-R)]^{2} \quad (1)$$

where C and m are constants dependent on the thickness and type of material, K_{env} is the factor that accounts for environment, and R is the stress ratio (minimum stress/maximum stress).

The constants C and m can be obtained for any material and thickness in the laboratory tests on simple specimens, e.g., center-cracked, compact. These constants, along with elastic stress intensity factors in a structure, can be used to predict fatigue crack growth life of a cracked aircraft structure.

The use of the J integral in fatigue crack growth prediction would require developing a crack growth equation similar to Eq. (1), which would have the form

$$\frac{da}{dn} = C_1 J_{max}^{m_1}[(J_{max} + J_{env})(1-R)]^{m_2} \quad (2)$$

The development of this type of equation would require obtaining constants C_1, m_1, m_2, and J_{env} from the test data. It would also necessitate nonlinear analysis of the test specimen with subsequent computation of J values. However, this extra effort may be avoided by a simplified procedure, which consists of the following steps:

1) Obtain the values of C, m, and K_{env} in a crack growth equation similar to Eq. (1) for the material and thickness under consideration from a simple laboratory specimen.

2) Perform a nonlinear analysis of the structure under consideration using finite-element analysis, assuming a Prandtl-Reuss material behavior.

3) Obtain J-integral values for various applied stress levels and crack lengths.

4) Compute the plasticity-corrected stress intensity factors K_I from the J integral values using the appropriate equation

$$J = \frac{1-\nu^2}{E}K_I^2 \quad \text{for plane strain}$$

$$J = \frac{K_I^2}{E} \quad \text{for plane stress} \quad (3)$$

The value of Young's modulus E is that which corresponds to the linear elastic behavior of the material.

These computed stress intensity factors are now a nonlinear function of applied stress, i.e., the normalized stress intensity factor $K/\sigma\sqrt{\pi a}$ is not a constant for a particular crack length but depends on the remote stress. In a linear elastic analysis, the normalized stress intensity factor $K/\sigma\sqrt{\pi a}$ is a constant for a particular crack length and does not depend on remotely applied stress.

5) Using the stress intensity factors obtained in step 4, and the crack growth equation in step 1, fatigue crack growth behavior can be predicted.

Test Specimens and Materials

Three specimen configurations with notch radii of 0.5, 1.5, and 3.0 in. (12.7, 38.1, and 76.2 mm) were selected to represent typical geometries found in an aircraft wing. The materials selected were 7075-T651 (0.402 in. (10.2 mm) thickness) and 7075-T7351 aluminum plate (0.52 in. (13.2 mm) thickness) for the 0.5 in. (12.7 mm) notch radius, and 7075-T7351 for the 1.5 and 3.0 in. (38.1 and 76.2 mm) radii. The test specimen configuration is shown in Fig. 1. The desired stress gradients at the uncracked notch radii were obtained by the positioning of loading holes. The required hole positions were obtained from stress analysis of the uncracked specimens. For the 0.5 in. (12.7 mm) radii specimens ($W = 6.0$ in. (152.4 mm) in Fig. 1), the required stress gradient was obtained by loading the specimen along the centerline ($e = 0$ in Fig. 1). For the 3.0 in. (76.2 mm) radius specimens ($W = 8.0$ in. (203.2 mm) in Fig. 1), the loading was applied off-center ($e = 1.5$ in. (38.1 mm) in Fig. 1) in order to simulate the required gradient.

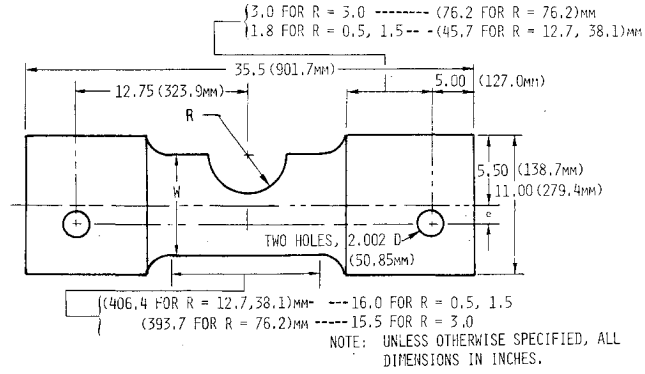

Fig. 1 Test coupon geometry: 0.50, 150, and 3.00 in. (12.7, 38.1, and 76.2 mm) radii.

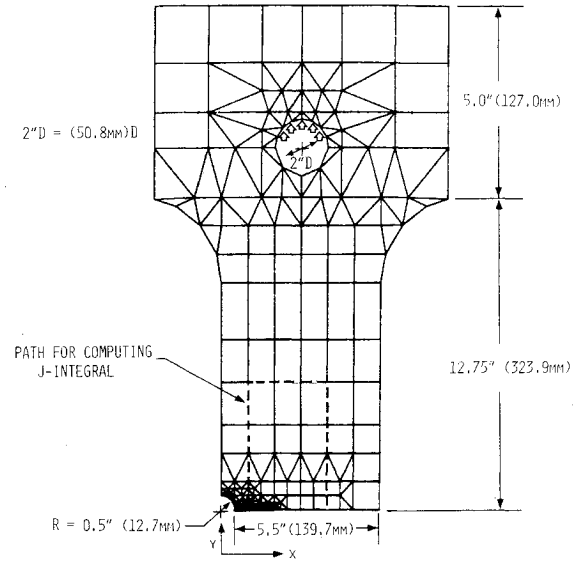

Fig. 2 NASTRAN finite-element model of 0.50 in. (12.7 mm) test coupon.

All tests were conducted at constant amplitude loading and frequency (0.1-0.2 Hz). All specimens were tested in laboratory air at a stress ratio of 0.1. The initial crack was created from a jeweler saw cut, and subsequently precracked to the required starting size.

Nonlinear Analysis with NASTRAN

The finite-element model of one-half of the specimen with a 0.5 in. (12.7 mm) radius is shown in Fig. 2. A fine mesh (Fig. 3) was provided around the hole and crack tip so that the stresses and displacements could be accurately computed. Rectangular and triangular elements (CQDMEM and CTRMEM) were used in a two-dimensional finite-element model. An element size of 0.05 in. (1.3 mm) was used around the hole and for small crack lengths [less than 0.2 in. (5.1

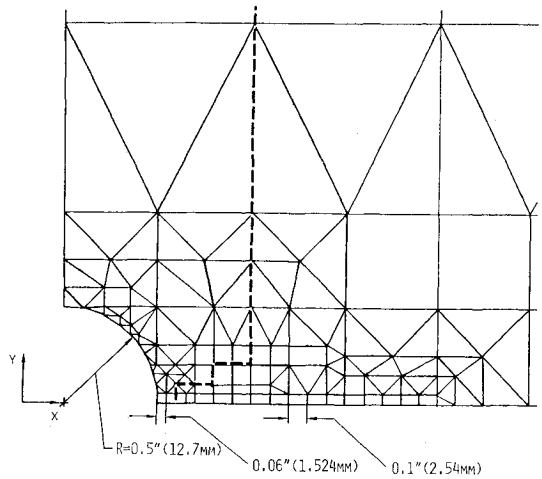

Fig. 3 Enlarged view of NASTRAN finite-element model in region of crack.

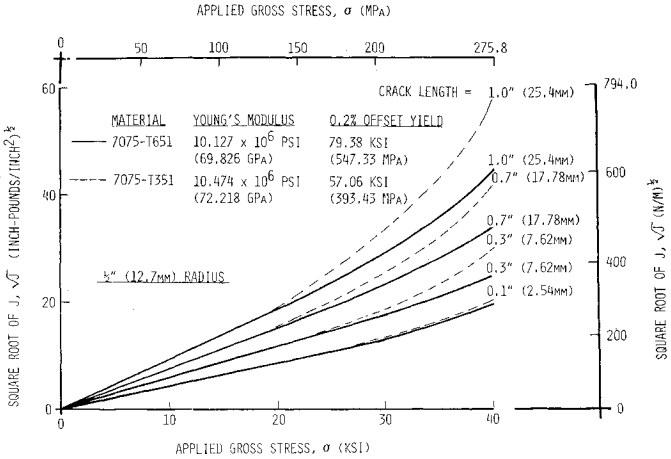

Fig. 4 Square root of J as function of applied stress, 0.50 in. (12.7 mm) radius.

mm)]. This element size was increased to 0.1 in. (2.5 mm) for longer crack lengths, as shown in Fig. 3.

The nonlinear analysis was carried out with NASTRAN as a piecewise linear analysis by putting the actual stress-strain curves of 7075-T651 and 7075-T7351 alloys in the computer program. The finite-element analysis was carried out for the 0.5 in. (12.7 mm) radius specimen at an applied remote stress of 10, 20, 30, and 40 ksi (68.95, 137.9, 206.84, and 275.79 MPa) for crack lengths of 0.1, 0.3, 0.7, and 1.0 in. (2.5, 7.6, 17.8, and 25.4 mm). The J-integral values are given by Ref. 5

$$J=\int_{\Gamma}\left(W\mathrm{d}y-\bar{T}\frac{\partial\bar{u}}{\partial x}\mathrm{d}s\right) \tag{4}$$

where Γ is any contour surrounding the crack tip traversing in a counterclockwise direction, W is the strain energy, $\bar{T}$ is the traction on Γ, and $\bar{u}$ is the displacement vector.

The details of J-integral computation and the path independent of the J integral for the piecewise linear analysis with NASTRAN are described in Refs. 6-8. It was not considered necessary to compute the J integral for more than one path. Therefore, only the one contour shown in Fig. 2 was used to compute the J-integral values.

The variation of the square root of J ($\sqrt{J}$) with applied stress for the two aluminum alloys (7075-T651 and 7075-T7351) is shown in Fig. 4 for the 0.5 in. (12.7 mm) radius specimen. The figure indicates that the nonlinear effects are observed at an applied stress as low as 20 ksi (137.9 MPa). For the same applied stress and crack length, the $\sqrt{J}$ values ob-

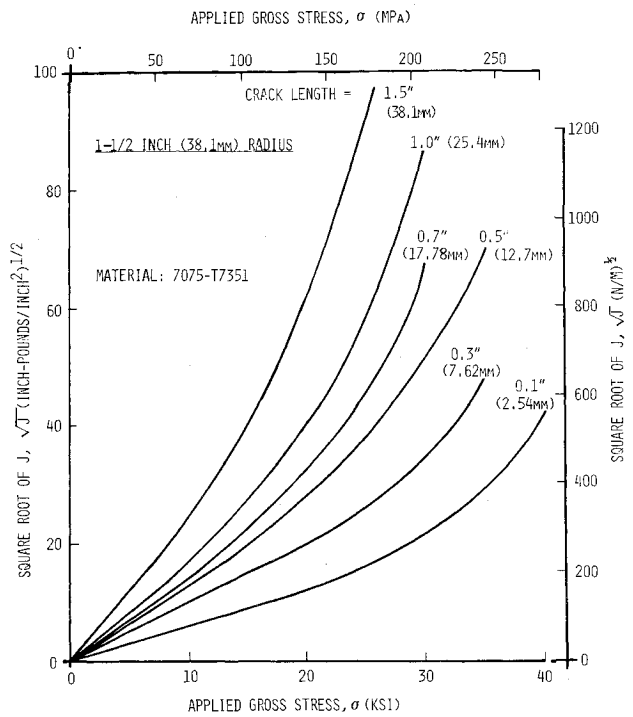

Fig. 5 Square root of J as function of applied stress, 1.50 in. (38.1 mm) radius.

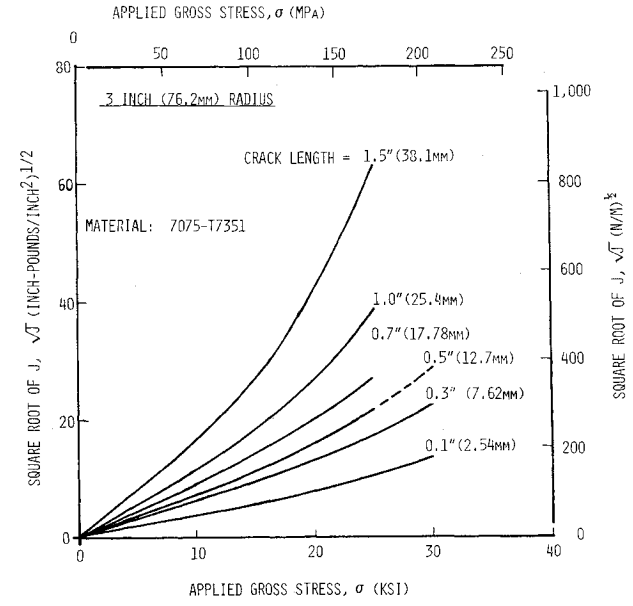

Fig. 6 Square root of J as function of applied stress, 3.00 in. (76.2 mm) radius.

tained for 7075-T7351 material are higher than those for 7075-T651 in the nonlinear range.

The variation of $\sqrt{J}$ with applied stress for 1.5 and 3.0 in. (38.1 and 76.2 mm) specimens is shown in Figs. 5 and 6, respectively. The nonlinear effects for 1.5 and 3.0 in. (38.1 and 76.2 mm) specimens are observed at applied stresses larger than 15 and 10 ksi (103.42 and 68.95 MPa), respectively.

The variation of $\sqrt{J}$ with crack length for various applied stresses for the 0.5 in. (12.7 mm) radius specimen (cross-plot of Fig. 4) is shown in Fig. 7. It is seen that at an applied stress of 10 ksi (68.95 MPa) nonlinear effects are not observed. For higher stresses, the extent of nonlinearity depends on the crack length.

The computed plastic zones for various crack lengths in the 0.5 in. (12.7 mm) radius specimen are shown in Fig. 8 at an

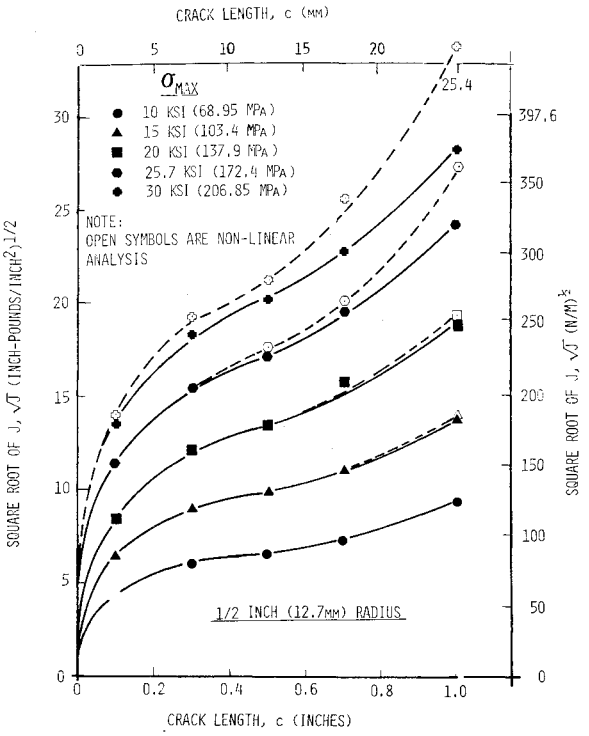

Fig. 7 Square root of J as function of crack length, 0.50 in. (12.7 mm) radius.

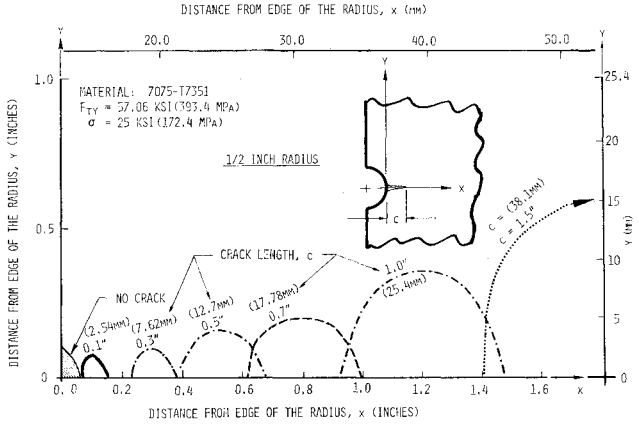

Fig. 8 Plastic zones for various crack lengths in 0.5 in. (12.7 mm) radius specimen.

applied stress of 25 ksi (172.37 MPa). Note the size of the plastic zone for the uncracked condition. It can be seen that the specimen goes plastic in the vicinity of the radius at an applied stress of 25 ksi (172.37 MPa).

Correlation between Analytical Predictions and Experimental Results: Through-the-Thickness Flaws

Linear elastic fatigue crack growth data for 7075-T7351 (0.52 in. (13.2 mm) thickness) and 7075-T651 (0.402 in. (10.2 mm) thickness) aluminum plate were obtained from compact specimens at a stress ratio of 0.10. Equation (1) was fitted to the data measured from these tests and a typical result for 7075-T651 material is shown in Fig. 9.

Plasticity-corrected stress intensity factors are obtained using Eq. (3) and curves of Figs. 4-7 for various crack lengths and applied stress levels for three different notch radii. Using these stress intensity factors and crack growth [Eq. (1)], the predicted crack growth life of one specimen with a 0.5 in. (12.7 mm) radius is shown in Fig. 10. The figure also shows the results of analytical predictions made with elastic stress intensity factors. The correlation between analytical

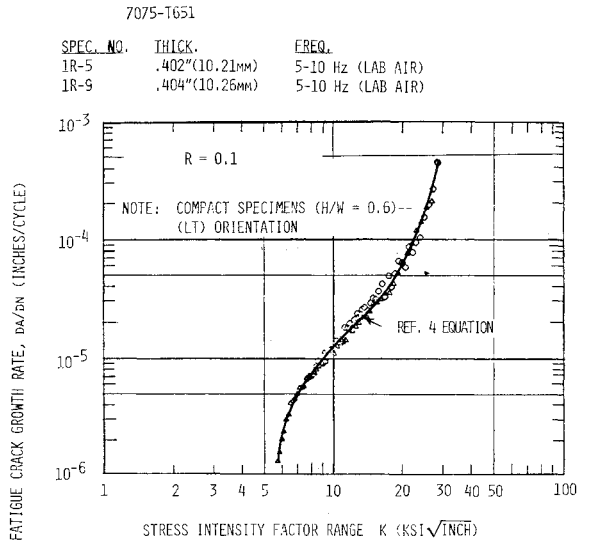

Fig. 9 Fatigue crack growth rate data for 7075-T651 aluminum.

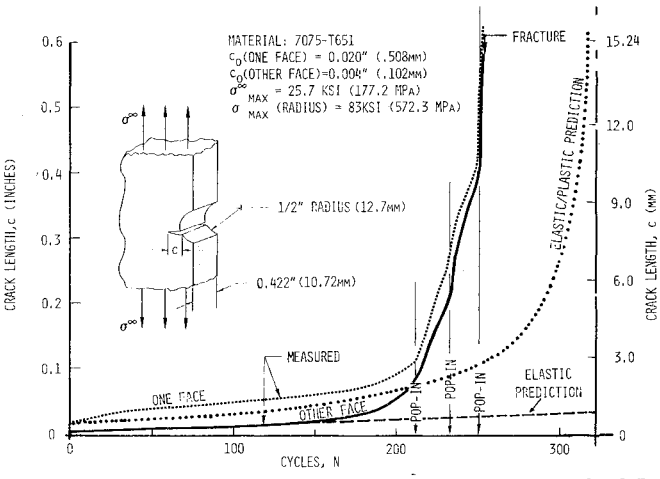

Fig. 10 Comparison of predicted and measured crack growth for 0.5 in. (12.7 mm) radius specimen.

Table 1 Comparison of predicted and observed results

Radius, in. (mm)	Material	Experimentally observed cycles to failure	Predicted cycles-to-failure nonlinear analysis
0.5 (12.7)	7075-T651	255	315
0.5 (12.7)	7075-T7351	1942	2200
1.5 (38.1)	7075-T7351	2472	2800
3.0 (76.2)	7075-T7351	535	468
3.0 (76.2)	7075-T7351	291	136

predictions made with plasticity-corrected stress intensity factors and experimentally observed crack lengths is good. The predictions made with elastic analysis are unconservative.

A comparison of predicted cycles to failure, using nonlinear analysis and experimentally observed cycles to failure for through-the-thickness crack specimens is shown in Table 1. It is seen that comparison between experimental results and predicted cycles, using nonlinear analysis is good, except for one specimen.

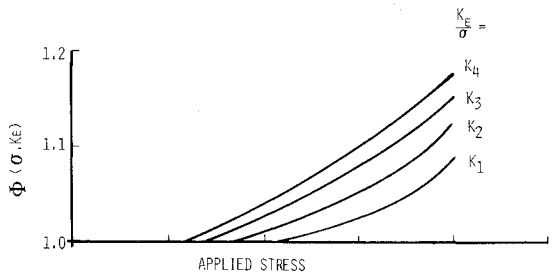

Fig. 11 Representation of plasticity-correction factor.

Application of the *J* Integral to Nonlinear Analysis of Surface Flaws

The relation between elastic stress intensity factors K_e and J integral (J_e) for elastic material behavior and plane stress conditions is given by

$$K_e = \sqrt{J_e E} \tag{5}$$

where E is Young's modulus for elastic behavior. We can define a plasticity-corrected stress intensity factor K_p as

$$K_p = \sqrt{J_p E} \tag{6}$$

where J_p is the value of the J integral for nonlinear material. Combining Eqs. (5) and (6)

$$K_p = K_e \sqrt{J_p / J_e} \tag{7}$$

For a particular structural and crack geometry, the values of K_e and J_e are readily determined. The value of J_p depends on the applied stress, crack length, and nonlinear behavior of the material. The value of J_p is obtained from the nonlinear analysis (e.g., finite element) of the crack geometry under consideration. For a particular material, Eq. (7) can be written as

$$K_p = K_e \varphi(\sigma, K_e) \tag{8}$$

where $\varphi(\sigma,K_e) = \sqrt{J_p/J_e}$ is the correction to be applied to the elastic stress intensity factors to account for the influence of plasticity. For a particular material, this influence depends on the applied remote stress and crack length. The value of $\varphi(\sigma,K_e)$ is obtained for through-the-thickness cracks using the nonlinear analysis discussed earlier. The variation of $\varphi(\sigma,K_e)$ with applied stress is schematically shown in Fig. 11 for various values of elastic stress intensity factors.

In applying the J-integral approach to part-through-the-thickness flaws, it is assumed that for the same value of applied remote stress and elastic stress intensity factor, the nonlinear effects on stress intensity factor for through-the-thickness flaws and part-through-the-thickness flaws are the same. Thus, it is assumed in Eq. (8) that $\varphi(\sigma,K_e)$ is the same for through-the-thickness and part-through-the-thickness flaws for a given material. The proposed nonlinear analysis of part-through and corner flaws will require the following steps:

1) Perform the nonlinear analysis of the structure under consideration for various lengths of through-the-thickness cracks at various applied stresses.

2) Compute the J-integral values for various crack lengths and applied stresses. From these values, obtain $\varphi(\sigma,K_E)$ using Eq. (8) for various values of applied stresses and elastic stress intensity factors (K_E/σ), as shown schematically in Fig. 1.

3) Obtain the elastic stress intensity factors (K_E/σ) for surface or corner flaws using any existing methodology (e.g., Ref. 9).

4) Using the elastic stress intensity factors for part-through-the-thickness flaws and applied stress, compute the plasticity-correction factor $\varphi(\sigma,K_E)$ from the curves obtained in step 2.

5) The plasticity-corrected stress intensity factor (K_p) for part-through flaws is given by the elastic stress intensity factor K_E (computed in step 3) multiplied by the plasticity correction $\varphi(\sigma,K_E)$ computed in step 4.

6) The stress intensity factors computed in step 5 are used in crack growth life predictions.

The variation of $\varphi(\sigma,K_E)$ with applied stress for a crack at a 0.5 in. (12.7 mm) radius in 7075-T7351 aluminum is shown in Fig. 12 for various values of elastic stress intensity factors. It is seen that the influence of plasticity increases with the increase in the stress intensity factor and applied stress.

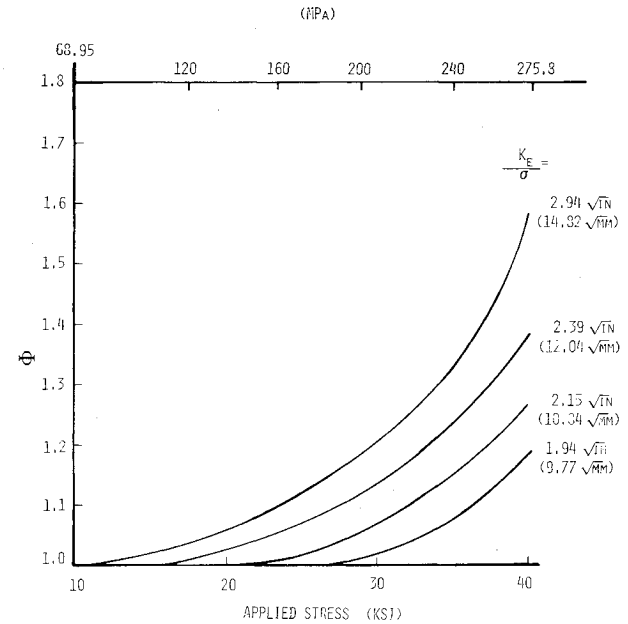

Fig. 12 Variation of plasticity-correction factor with applied stress for cracks at 0.5 in. (12.7 mm) radius in 7075-T73 aluminum.

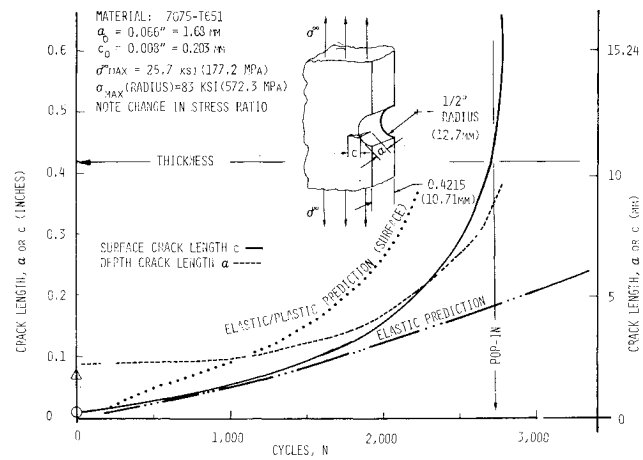

Fig. 13 Comparison of predicted and measured crack growth for specimen with 0.5 in. (12.7 mm) notch radius and part-through flaw.

Test Verification Program for Part-Through-the-Thickness Flaws

Two notch radii, 0.5 and 3.0 in. (12.7 and 76.2 mm), were selected to represent dimensions typically found in aircraft wings. The aluminum alloys selected were 7075-T651 and 7075-T7351 for the 0.5 in. (12.7 mm) notch radius and 7075-T7351 for the 3.0 in. (76.2 mm) notch radius. The test specimen geometry and loading hole position were the same as discussed for through-the-thickness flaws. Four tests were

Table 2 Comparison of predicted and observed cycles to failure

Radius, in. (mm)	Maximum stress at notch radius, ksi (MPa)	Material	Experimentally observed cycles to failure	Predicted cycles to failure (nonlinear analysis)
0.5 (12.7)	83.0 (572.3)	7075-T651	2776	2100
0.5 (12.7)	65.6 (452.3)	7075-T7351	7713	7100
3.0 (76.2)	63.5 (435.4)	7075-T7351	2424	2781
3.0 (76.2)	63.5 (435.4)	7075-T7351	3279	2144
3.0 (76.2)	58.5 (403.3)	7075-T7351	1625 flights[a]	1603 flights[a]

[a] Spectrum, 1203 flights/1000 h.

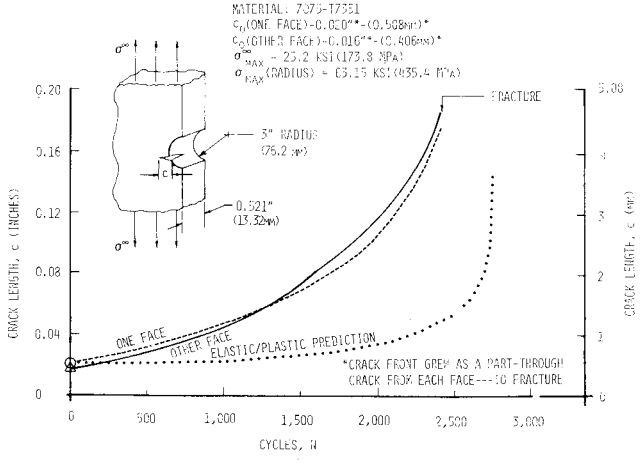

Fig. 14 Comparison of predicted and measured crack growth for 3 in. (76.2 mm) specimen with part-through crack.

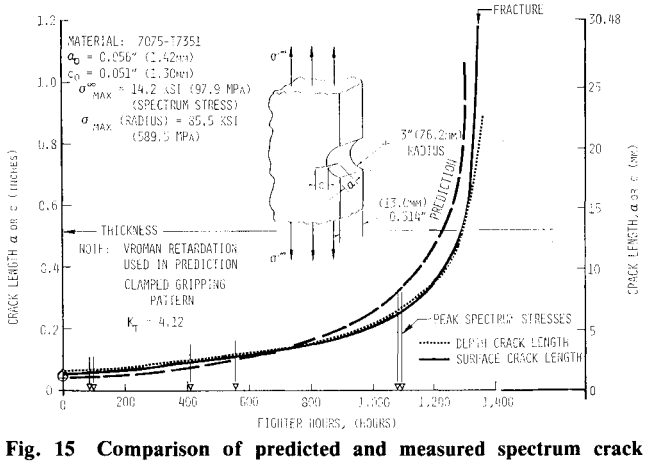

Fig. 15 Comparison of predicted and measured spectrum crack growth for 3.0 in. (76.2 mm) radius specimen with part-through crack.

conducted under constant amplitude loading at minimum stress/maximum stress ratio R of 0.1. One specimen (7075-T7351) with a 3.0 in. (76.2 mm) notch radius was tested to spectrum loading. The peak spectrum stress was selected to obtain a 58.5 ksi (403.35 MPa) maximum stress (the 0.2% offset yield being 57.7 ksi (397.83 MPa) at the 3.0 in. (76.2 mm) radius with no cracks. This specimen differed in loading arrangement from the other 3.0 in. (76.2 mm) radii specimens discussed for through-the-thickness flaws. Clamped gripping (rather than pin loading) was used to handle the compressive spectrum loads.

Correlation between Analytical Predictions and Experimental Results for Part-Through-the-Thickness Flaws

The fatigue crack growth data obtained on compact specimens in the elastic range and the plasticity-corrected stress intensity factors, discussed earlier, were used to predict crack growth behavior of part-through-the-thickness flaws. Typical crack growth data for the 7075-T651 specimen with a 0.5 in. (12.7 mm) notch radius are shown in Fig. 13. The figure also shows the results of analytical predictions made with plasticity-corrected stress intensity factors and elastic stress intensity factors. The correlation between the analytical predictions made with plasticity correction and the experimentally observed results is good. The predictions made with elastic material behavior are unconservative.

Crack growth data for the 7075-T7351 specimen with a 3.0 in. (76.2 mm) notch radius are shown in Fig. 14. For this case, the elastic-plastic analysis predicts crack growth life about 15% higher than actual specimen life.

The observed and predicted crack growth behavior of specimens tested under spectrum loading is shown in Fig. 15. The predictions were made using the NORCRACK computer program with the Vroman[10] retardation parameters in the analysis. The stress used for the analysis was obtained from that measured on the specimen itself using strain gages. The stress intensity factors used were based on the nonlinear behavior discussed earlier. As seen in the figure, both the crack growth rate and failure predictions are excellent.

A comparison of predicted cycles to failure, using nonlinear analysis, and experimentally observed cycles to failure for various part-through-the-thickness crack specimens are shown in Table 2. Except for one 3.0 in. (76.2 mm) radius specimen, the predicted life is within about 20% of the actual life.

Conclusions

1) The fatigue crack growth behavior in a nonlinear stress field caused by local stress concentrations cannot be reliably predicted with LEFM methods. LEFM predicts slower crack growth than that actually observed.

2) Modified elastic-plastic stress intensity factors, based on the J integral, have been successfully used to predict crack growth life.

3) 7075-T7351 aluminum exhibits considerably larger nonlinearity than 7075-T651. The J-integral values for 7075-T7351 aluminum are larger than those for 7075-T651 for the same applied stress and crack length.

4) Modified elastic stress intensity factors for part-through-the-thickness flaws, based on J-integral values for through-the-thickness flaws, have been used successfully to predict crack growth life under constant amplitude and spectrum loading for a small number of specimens tested.

Acknowledgment

The work reported in this paper was sponsored by the San Antonio Air Logistic Command.

References

[1] Broek, D., "The Propagation of Fatigue Cracks Emanating from Holes," National Aerospace Laboratory NLR, The Netherlands, Rept. NLR TR 72134U, 1972.

[2] Kang, S.T. and Liu, H.E., "The Effect of Prestress Cycles on Fatigue Crack Growth: An Analysis of Crack Growth Mechanism," *Engineering Fracture Mechanics,* Vol. 6, 1974, pp. 631-638.

[3] Schijve, J., "The Effect of Prestrain on Fatigue Crack Growth and Crack Closure," *Engineering Fracture Mechanics,* Vol. 8, 1976, pp. 575-581.

[4] Fitzgerald, J.H., "Empirical Formulation for the Analysis and Prediction of Trends for Steady-State Fatigue Crack Growth Rates," *Journal of Testing and Evaluation,* Vol. 5, No. 5, pp. 343-353.

[5] Rice, J.R., "A Path Independent Integral and Approximate Analysis of Strain Concentration by Notches and Cracks," *Transactions of ASME, Journal of Applied Mechanics,* June 1968, pp. 379-386.

[6] Ratwani, M.M. and Wilhem, D.P., "Development and Evaluation of Methods of Plane Stress Fracture Analysis—A Technique for Predicting Residual Strength of Structure," AFFDL-TR-73-42, Part II, Vol. I, Aug. 1977.

[7] Ratwani, M.M. and Wilhem, D.P., "Development and Evaluation of Methods of Plane Stress Fracture Analysis—Application of Residual Strength Prediction Technique to Complex Aircraft Structures," AFFDL-TR-73-42, Part III, Aug. 1977.

[8] Wilhem, D.P., Ratwani, M.M., and Zielsdorff, G.F., "A *J*-Integral Approach to Crack Growth Resistance for Aluminum, Steel and Titanium Alloys," *ASME Journal of Engineering Materials and Technology,* April 1977, pp. 97-104.

[9] Newmann, J.C., "Fracture Analysis of Surface and Through-Cracked Sheets and Plates," *Engineering Fracture Mechanics,* Vol. 3, 1973, pp. 667-689.

[10] "Crack Propagation Analysis by Vroman's Model—Computer Analysis Summary, Program EFFGRO," Feb. 1972, Los Angeles Div., Rockwell International, NA-72-94.